Original Research Article for *Chem. Phys. Rev. (CPR) – further revised 2024*

Ultrafast planarization of photoexcited ligands in metal-organic frameworks gates charge transfer to promote photocatalysis

Logan S. Lancaster,[1] Taylor D. Krueger,[1] Cheng Chen,[1] Emmanuel Nyela Musa,[2] Jacob M. Lessard,[2] Nan-Chieh Chiu,[2] Makenzie T. Nord,[1] Kyriakos C. Stylianou,[2] and Chong Fang[1,a)]

[1] Department of Chemistry, Oregon State University, 153 Gilbert Hall, Corvallis, Oregon 97331, United States

[2] Materials Discovery Laboratory (MaD Lab), Department of Chemistry, Oregon State University, 153 Gilbert Hall, Corvallis, Oregon 97331, United States

[a)]Author to whom correspondence should be addressed: Chong.Fang@oregonstate.edu

Abstract

Metal-organic frameworks (MOFs) have emerged as a highly tunable class of porous materials with wide-ranging applications from gas capture to photocatalysis. Developing these exciting properties to their fullest extent requires a thorough mechanistic understanding of the structure-function relationships. We implement an ultrafast spectroscopic toolset, femtosecond transient absorption (fs-TA) and femtosecond stimulated Raman spectroscopy (FSRS), to elucidate the correlated electronic and vibrational dynamics of two isostructural 1,3,6,8-tetrakis(*p*-benzoic acid)pyrene (TBAPy)-based MOFs, which manifest drastically different photocatalytic behaviors. Systematic comparisons between the M^{3+}-TBAPy MOFs and bare ligands in various environments reveal the unproductive dimer formation in Al-TBAPy, whereas Sc-TBAPy is dominated by a catalytically active charge-transfer (CT) process. Two ground-state FSRS marker bands of the TBAPy ligand at ~1267 and 1617 cm^{-1} probe the chromophore environment at thermal equilibrium. For comparison, the excited-state FSRS of Sc-TBAPy suspended in neutral water unveils a key ~300 fs twisting motion of the TBAPy peripheral phenyl groups toward planarity, promoting an efficient generation of CT species. This motion also exhibits high sensitivity to solvent environment, which can be a useful probe; we also showed the CT variation for ultrafast dynamics of Sc-TBAPy in glyphosate aqueous solution. These new insights showcase the power of table-top tunable FSRS methodology to delineate structural dynamics of functional molecular systems in action, including MOFs and other photosensitive "nanomachines". We expect the uncovered ligand motions (ultrafast planarization) to enable the targeted design of new MOFs with improved CT state characteristics (formation and lifetime) to power applications including photocatalysis and herbicide removal from waterways.

1. Introduction

Metal-organic frameworks (MOFs) represent a promising class of materials, garnering substantial interest over the past three decades with more than 100,000 MOFs reported to date.[1,2] The inherent tunability of MOFs in combination with extremely high surface area have propelled MOFs into versatile use across multiple application areas from gas capture to environmental remediation.[3-6] MOFs assembled using photoactive ligands are of particular interest since the highly ordered, dense packing of ligands can promote efficient light harvesting and energy transfer.[7-11] Particularly, in combination with the catalytically active metal sites, such ligands can enable the formation of powerful and tunable photocatalysts.[12,13] Among the vast number of MOFs that have been synthesized, only a small cadre of them are suitable for photocatalytic applications, which require strong visible light absorption and efficient charge separation.[5,14,15] Tetra-functionalized pyrene ligands have since been synthesized into a variety of metal-organic frameworks,[3,8,16] motivated by the strong visible absorption, long excited-state lifetime, and high fluorescence quantum yield (FQY) of pyrene.[17-20]

The most studied pyrene-based ligand is 1,3,6,8-tetrakis(*p*-benzoic acid)pyrene as TBAPy linkers inside MOFs. Numerous TBAPy-MOFs have been studied and engineered for their use in photocatalysis toward hydrogen fuel.[12,13,21,22] TBAPy-MOFs form several topologically unique crystal structures depending on synthesis conditions and metal-ion identity, thereby allowing detailed examination of the impact of linker arrangement.[23-26] These studies revealed the pyrene-derived excimers with long excited-state lifetimes (>30 ns)[27] and shorter-lived MOF excimers such as ~8 ns in $[In_2(OH)_2(TBAPy)]$ (ROD-7),[23] wherein the degree of excimer formation is controlled by the inter-linker distances and angles; such excimers have notable implications for the optical properties and photocatalytic behaviors of MOFs (see below).

Our recent study of four isostructural TBAPy-MOFs utilizing different metal nodes demonstrated promising photocatalytic performance of Sc-TBAPy (note that we may omit the phrase MOF for brevity; Al- or Sc-TBAPy refer to the MOFs under study) for the effective adsorption and photodegradation of the herbicide glyphosate (GP) with high specificity (e.g., only Sc-TBAPy shows selectivity toward the formation of nontoxic species via oxidation of GP, while reducing H^+ to produce H_2).[6,28] Compared with other M^{3+}-TBAPy MOFs, Sc-TBAPy displays a substantially increased bifunctionality in hydrogen generation and GP degradation, resulting from its markedly enhanced CT character. A previous study of Sc-TBAPy suggested that although ligand-to-metal charge-transfer (LMCT) is not favored, the ligand lowest unoccupied molecular orbital (LUMO, pyrene π^* states) and the Sc-nodes' *d*-orbitals have similar energies, resulting in a ligand-centered excitation with enhanced electron density on the peripheral benzenes and Sc-nodes compared to other metals.[13] The interactions between metal and ligand orbitals in Sc-TBAPy support higher electron mobility and make this material unique among M^{3+}-TBAPy frameworks. The structure-function relationships governing the exceptional photocatalytic performance of Sc-TBAPy are largely opaque; therefore, ultrafast spectroscopic measurements can offer unique insights into the catalytic pathways of pyrene-based MOFs. Moreover, fundamental knowledge of these pathways can guide future development of new photocatalytic MOFs through the targeted ligand engineering (see discussions in Section 2.5 below).

In this work, we explore the photoactivity of two TBAPy-MOFs, Al-TBAPy and Sc-TBAPy (see Fig. 1a for TBAPy, and Fig. 1b, d for the MOF structures), using steady-state electronic and vibrational spectroscopy in conjunction with transient measurements. Ground-state femtosecond stimulated Raman spectroscopy (GS-FSRS) reveals different linker environments (e.g., solvent access, excimer formation) in the two MOFs despite the conserved structure, with considerably

increased inter-linker interactions in Al-TBAPy vs. Sc-TBAPy. On the mechanistic front with a focus on structural dynamics, femtosecond transient absorption (fs-TA) spectroscopy in tandem with excited-state (ES)-FSRS track the initial excited-state relaxation inside MOFs and unveil a key ultrafast planarization step of the ligand modulating CT process. On the more application side, fs-TA measurements of Sc-TBAPy under pseudo-photocatalytic conditions (1.5 mM aqueous GP solution, 400 nm excitation) demonstrates a more pronounced quenching step of the CT band on the few picoseconds (ps) timescale than in pH 7 water (i.e., without GP); this finding substantiates the functional role of an ultrafast CT process in GP removal/degradation downstream.

2. Results and Discussion

2.1. Steady-state electronic spectra of bare ligands and MOFs in various solutions

Both MOFs possess the same crystal structure (Fig. 1b, d) formed from 1D chains of metal-oxo clusters, each bound to four TBAPy linkers that are totally eclipsed, with pyrene cores stacked directly above the neighboring layer. The peripheral benzoate groups form a total of eight bonds to the metal ions with an equilibrium dihedral angle $\tau \approx 75°$ between the pyrene core and the benzene ring.[3] These MOFs contain three distinct pores (Fig. S1, Supplementary Material), which allow guest molecules to access the vast surface area of these functional materials.[4,13]

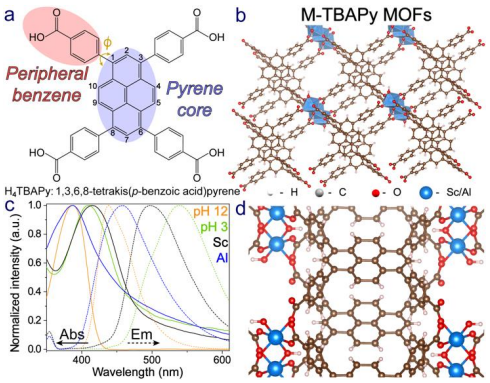

FIG. 1. Structural diagrams and steady-state electronic spectroscopy of M-TBAPy MOFs and bare ligands. The (a) ligand/linker structure and (b, d) MOF crystal lattice structure diagrams with different perspectives are shown, along with (c) steady-state absorption (Abs, solid lines) and emission spectra (Em, dashed lines) for Sc-TBAPy (black) and Al-TBAPy (blue) MOFs in pH 7 aqueous solution, and dilute bare ligands in pH 12 (orange) and pH 3 (green) aqueous solution. In panel a, the core (violet) and peripheral (maroon) regions of the organic linker H_4TBAPy are marked with the semi-transparent colored ellipses, and the phenyl-ring-twist angle is shown as ϕ.

Steady-state absorption and emission spectra of both MOFs suspended in pH 7 water show clear similarities when compared with bare TBAPy ligands (Fig. 1c), in accord with the expected ligand-derived photoactivity of MOFs. Both MOFs display broadened absorption and emission profiles as a result of the solid-state nature (e.g., conformational heterogeneity) of the framework. Interestingly, while Al-TBAPy has a similar absorption peak as bare ligands (in pH 12 aqueous solution) at ~387 nm, the absorption peak of Sc-TBAPy appears at ~410 nm, similar to aggregated ligands in pH 3 aqueous solution. Except the pH 12 case, all the absorption spectra show sloping tails toward the long-wavelength region (>450 nm) largely due to Mie scattering from the suspended particles that are similar or larger than the wavelength of visible light, likely containing some low-energy absorption features as well. In the case of aggregated ligands, two low-energy shoulder peaks are observed around 450 and 490 nm, which are dramatically enhanced at higher ligand concentrations (Fig. S2a), suggesting their origin from dimeric aggregates as reported in several tetraphenyl-pyrene derivatives in solid state and solution.[29,30] In contrast, the MOFs reveal weak evidence of dimer formation at higher concentrations (Fig. S2b), mostly consistent with the incorporated organic linkers in well-defined locations of the framework (Fig. 1b, d).

Despite the clearly shifted absorption and emission profiles of the two MOFs, the Stokes shifts are nearly identical at ~4000 cm^{-1} for Al- and Sc-TBAPy. This value is greater than that of the free ligand (3000 cm^{-1}) but considerably less than the aggregated ligand (5900 cm^{-1}), the latter case being consistent with the formation of dimers with low-energy emission features. The conserved Stokes shift between the MOFs suggests that they experience similar relaxation within their emissive states; meanwhile, the red-shifted absorption and emission peaks of Sc-TBAPy arise from solvent interactions which prompt structural deformation of the framework, as previously observed for In-TBAPy, rather than the ligand aggregation/dimer formation.[3]

To examine the solvent dependence of electronic absorption, measurements of both MOFs in dimethylformamide (DMF) and acetonitrile (ACN) were compared with those in aqueous solution (Fig. S3), showing that the Al-TBAPy absorption peak is largely conserved (387–390 nm) between solvents. In contrast, Sc-TBAPy shows a ~410 nm absorption peak in both water and ACN but a blue-shifted peak to 386 nm in DMF, closely matching the free ligand in pH 12 aqueous solution and Al-TBAPy (Fig. 1c). These results indicate that the solvent environment directly impacts the ligand/linker optical properties via the induced structural deformation inside the framework, leading to solvent-dependent absorption peaks with a sensitive relationship between solvent and the linker local environment in Sc-TBAPy (Fig. S3a). Previous studies have suggested that at relatively low loading, water preferentially occupies the pores closest to the metal nodes, near the peripheral phenyl groups (see Pore 1 in Fig. S1).[13,31] The proposed localization of the Sc-TBAPy excitation to these peripheral aromatic rings without significant dimeric interactions may thus contribute to the observed sensitivity of Sc-MOF versus Al-TBAPy to the solvent environment.

The FQY values of bare ligands were measured in solvents, which can be compared with an apparent FQY for MOFs (see Supplementary Material). As the MOFs are insoluble, this apparent

FQY cannot be interpreted quantitatively; nevertheless, it enables a qualitative comparison of the fluorescence efficiency of these materials. For example, the fluorescence of Al-TBAPy is stronger than Sc-TBAPy, with our measured FQYs of Al-TBAPy (0.162) and Sc-TBAPy (0.081) in ACN, consistent with the photoluminescence lifetime trend observed at ~500 nm in a previous report.[13] Since both materials emit from their constituent ligands and undergo similar excited-state relaxation, the reduced fluorescence efficiency of Sc-TBAPy implies additional nonradiative decay pathways (e.g., which can be useful for photocatalytic reactions such as H_2 generation and the herbicide removal from water, see below) in Sc-TBAPy versus Al-TBAPy.[28]

2.2. Time-resolved electronic spectra unveil a prominent charge-transfer state with a preparatory ligand peripheral-ring-twisting motion of M^{3+}-TBAPy MOFs in water

To shed light on relaxation pathways in these MOFs, we employed fs-TA spectroscopy to track transient electronic dynamics starting from time zero of photoexcitation. The experimental spectra of M^{3+}-TBAPy MOFs (M=Sc, Al) can be compared with bare ligands under basic and acidic conditions, representing the solvated and aggregated cases, respectively (Fig. 2). In particular, the solvated TBAPy ligands display a broad excited-state absorption (ESA) band with a notable ~700 nm peak, likely due to an $S_1 \rightarrow S_N$ transition (Fig. 2a).[17,25,32] The negative band below 500 nm can be assigned to stimulated emission/SE ($S_1 \rightarrow S_0$ transition), consistent with $TBAPy^{4-}$ fluorescence in this range (Fig. S4a), while no clear ground-state absorption occurs above ~450 nm (Fig. 1c).

For aggregated ligands, the ESA band is red-shifted while a broad negative feature extending beyond 600 nm dominates the spectrum throughout the detection time window of ~1 ns (Fig. 2b). The broadening of both positive and negative features is indicative of delocalized excitons, facilitated by π-π overlap of the neighboring linkers.[33] The overall signal intensity decrease from free ligands (Fig. 2a) to aggregated ligands (Fig. 2b) reflects a reduced oscillator strength of the S_1

transitions due to aggregation. The two strong negative bands around 500 and 555 nm are likely SE features; however, some ground-state absorption extends above 500 nm due to the dimeric aggregates (see Figs. S2a and S4b), hence ground-state bleaching (GSB) from certain species could contribute to the TA signal to some extent. These results are corroborated by our previous report comparing the solvated and aggregated TBAPy ligands in DMF and ACN, respectively.[28]

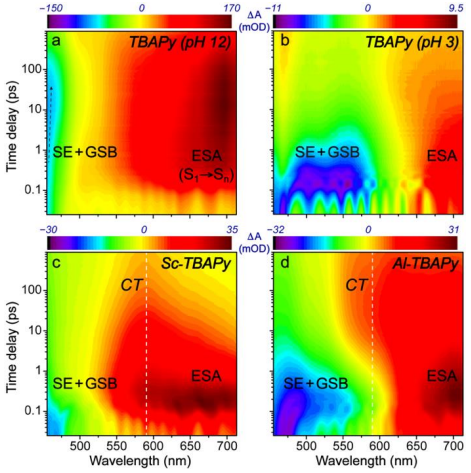

FIG. 2. Transient electronic dynamics of bare ligands and MOFs after 400 nm excitation. Contour plots of fs-TA spectra for TBAPy ligands in (a) pH 12 and (b) pH 3 aqueous solution, and (c) Sc-TBAPy and (d) Al-TBAPy MOFs suspended in pH 7 aqueous solution. The ground-state bleaching/stimulated emission (GSB/SE) and excited-state absorption (ESA) bands are labeled. In panels c and d, vertical dashed lines denote the nascent CT bands at ~590 nm in the MOFs. The intensity colorbars in the milli-optical density (mOD) unit are shown above each corresponding plot. The black tilted arrow highlights the negative peak redshift below ~500 nm in panel a.

The fs-TA spectra of both MOFs in water (Fig. 2c, d) also feature strong ESA bands and blue SE/GSB bands; however, the difference between the two MOFs is conspicuous. Al-TBAPy yields

a negative signal reminiscent of the aggregated ligands, extending up to ~600 nm (Fig. 2d), while Sc-TBAPy has a substantially broadened ESA band peaking around 660 nm (Fig. 2c). The broad negative features apparent in Al-TBAPy imply some aggregate-like interactions between the linker molecules within Al-TBAPy. In contrast, Sc-TBAPy does not display any pronounced negative features, and instead develops a long-lived band around 590 nm which dominates the transient spectra after ~1 ps (see the white dashed line in Fig. 2c). A similar band occurs in Al-TBAPy, albeit with a substantially delayed onset, becoming prominent only after ~5 ps. This marker band can be attributed to a charge-transfer (CT) state of the MOFs, in accord with reports of CT states observed in other TBAPy-MOFs[22,24] as well as the absorption spectra of radical TBAPy ions.[34]

Informed by the aforementioned solvent dependence of ground-state electronic spectra, further fs-TA experiments were conducted in organic solvents DMF and ACN to examine the CT process (Fig. S5). The results show a delayed onset and substantially reduced intensity of the CT band in Sc-TBAPy (Fig. S5a, c), while the CT band becomes almost undetectable in Al-TBAPy (Fig. S5b, d). The profound CT-band enhancement in water versus lower-polarity solvents confirms the polar nature of this state, which rises within the cross-correlation time of the setup (~100 fs) for Sc-TBAPy in water (Fig. 2c). Regarding control measurements for bare TBAPy ligands in DMF and in ACN, the resulting fs-TA spectra[28] bear striking similarity to the pH 12 and 3 aqueous solution cases in Figure 2a and 2b, respectively, indicating that solvation, not protonation, governs the major spectral differences observed for TBAPy ligands between the two pH conditions.

The electronic dynamics of contrasting samples were analyzed via global fitting in Glotaran (Fig. 3, also see SM text) to systematically extract the relevant timescales (see Table 1). The solvated ligands (Fig. 3a), as the simplest case, provide the foundation for understanding the MOF behaviors. Following an initial ultrafast (τ_1<100 fs) rise of both ESA and SE features (i.e.,

molecular motions out of the Franck-Condon region),[35,36] two components (τ_2=1.2 ps, τ_3= 6 ps) exhibit a continual rise of the 700 nm ESA band, accompanied by the rise and redshift of the blue SE band (see the tilted dashed line in Fig. 2a, while the adjacent ESA band also rises) which tracks relaxation dynamics of the TBAPy fluorescence state (e.g., chromophore conformational change, solvent reorganization).

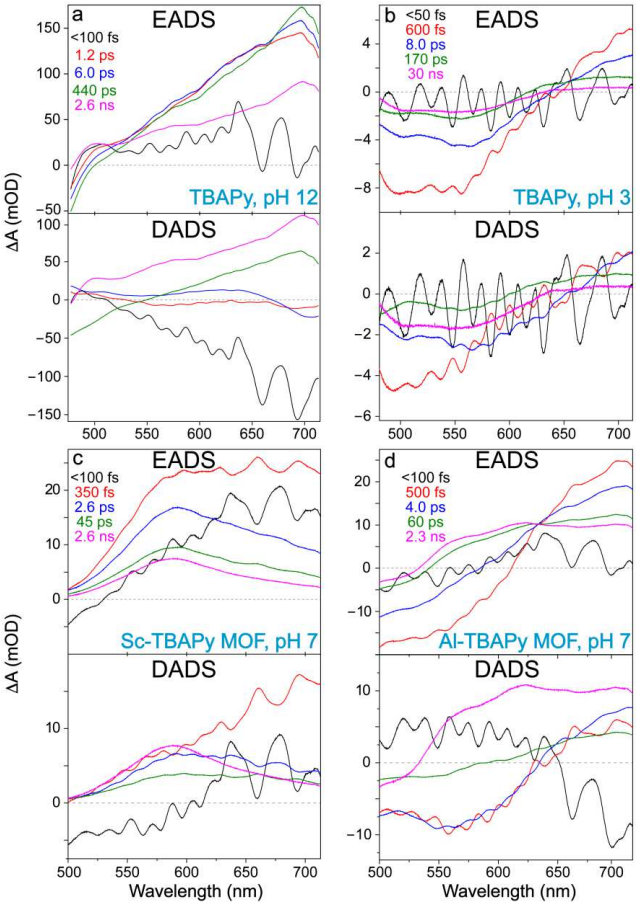

FIG. 3. Global fitting results for fs-TA spectra. The evolution-associated difference spectra (EADS, top) and decay-associated difference spectra (DADS, bottom) for transient electronic

spectra of bare TBAPy ligands in (a) pH 12 and (b) pH 3 aqueous solution compared with (c) Sc-TBAPy and (d) Al-TBAPy MOFs suspended in pH 7 aqueous solution. The lifetimes associated with each component are color-matched with the corresponding traces and listed for each sample. The zero milli-optical density (mOD) is shown as the horizontal gray dashed line in each panel. DADS are provided due to the potential for the ligand inhomogeneity at thermal equilibrium.

TABLE 1. Lifetimes retrieved from global analysis of fs-TA data collected for Sc- and Al-TBAPy MOFs in three solvents as well as bare TBAPy ligands in six solvents using the 900 ps setup.

Sample	Solvent	τ_1 (fs)	τ_2 (fs)	τ_3 (ps)	τ_4 (ps)	τ_5 (ns)
Sc-TBAPy	ACN	40	550	4.8	41	0.87
	DMF	80	600	6.0	55	1.4
	water (pH 7)	60	350	2.6	45	2.6
Al-TBAPy	ACN	60	600	6.8	50	1.2
	DMF	60	600	6.0	50	1.9
	water (pH 7)	50	500	4.0	60	2.3
TBAPy	water (pH 12)	90	1200	6.0	440	2.6
	water (pH 12) +glycerol	50	900	11.4	750 [a]	–
	water (pH 3)	50	600	8.0	170	30
	DMF	70	400	7.5	320	2.1
	ACN	40	670	10	290	35
	DMSO	100	350	9.3	–	1.3
	DMSO+glycerol	100	1900	31	–	1.3

[a] The long-time decay in this dataset is shortened likely due to experimental (alignment) issues.

Notably, τ_2 is shortened from ~1 ps in water to 350 fs in DMSO (Fig. S4d, e), demonstrating a higher solvent sensitivity than the other time constants. The ~1 ps component closely matches the solvation time of water;[37-39] however, the solvation time of DMSO is ~2 ps and thus τ_2 cannot be assigned simply to solvation.[20,40] The ESA band intensity rise associated with τ_2 implies twisting of the phenyl groups to a more planar configuration, which has been hypothesized to

increase the $S_1 \rightarrow S_N$ transition oscillator strength in pyrene derivatives with aromatic substituents.[17] Similar planarization events were observed for aromatic compounds including tetraphenyl ethylene with time constants of several hundreds of fs to ps.[41-43] This component tracks the peripheral phenyl ring-twists toward planarity in water (pH 12), which requires solvent reorganization due to strong electrostatic interactions between the deprotonated COO^- groups and water molecules. For comparison, DMSO lacks any H-bond donating capability which diminishes the dependence of this solute twist on solvent matrix, thus allowing a relatively fast motion toward planarization of TBAPy in DMSO. A complete planarization is not feasible due to sterics,[43] supported by our calculations using density functional theory (DFT) and time-dependent DFT (see Section 2.4 below); however, the equilibrium geometry in the excited state (away from Franck-Condon region) as predicted by TD-DFT calculations shows a ~10–15° twist of the peripheral rings toward planarity with respect to the ligand core.

The hundreds of ps time constant (τ_4) entails a substantial decay of both SE and ESA bands, likely through large-scale conformational changes, although it may be related to excimer formation that quenches the monomer excited states.[23] The final time constant (τ_5=2.6 ns) is similar to the reported value for TBAPy monomers in dilute DMF solution[23] and can be assigned to the apparent fluorescence lifetime of the deprotonated ligand chromophore. The aggregated ligands display a substantially extended lifetime of ~30 ns (Fig. 3b), confirming the presence of pyrene dimers.[27]

Both MOFs' fs-TA spectra are well fit using time constants comparable to bare ligands. However, τ_4 is drastically shortened from ~400 ps for free ligands to 45 and 60 ps for Sc-TBAPy and Al-TBAPy MOFs, respectively (Fig. 3c,d), which implies enforced rigidity of the frameworks that can restrict the linkers' large-scale conformational changes and/or the excimer formation and decay dynamics.[44] Importantly, Sc-TBAPy manifests a pronounced solvent-dependent change in

the longest lifetime τ_5: ~870 ps in ACN, 2.6 ns in water, with DMF at an intermediate value of 1.4 ns (Table 1).[28] In contrast, while Al-TBAPy shows a similar lifetime increase between ACN and DMF, only a modest increase is seen in water. Finally, though the overall excited-state lifetime of Sc-TBAPy is extended in water, the early dynamics are accelerated with considerably shortened τ_2 and τ_3 in water versus other solvents. The same trend holds for Al-TBAPy but to a lesser extent. The coupled acceleration of the sub-ps and ps components is directly correlated with prolonged excited-state lifetimes attributed to CT state, indicating that these time constants (τ_2 and τ_3) report on the formation of the CT state. The enhanced CT formation within the Sc-framework contributes to its lower FQY (i.e., the radiative pathway, see Section 2.1) and shorter excited-state lifetimes in DMF and ACN than Al-TBAPy (Table 1). This result contradicts conventional wisdom that longer excited-state lifetimes lead to higher catalytic efficiency; instead, the mobility and activity of the photogenerated excitons on ultrafast timescales, prior to fluorescence and other long-time energy relaxation involving free carriers,[45,46] are crucial for the enhanced performance of Sc-TBAPy. In other words, the correlated electronic and structural dynamics of the photoexcited moieties such as the organic ligands in MOFs need to be characterized for a more complete understanding of the MOF functionality, particularly regarding the TBAPy peripheral phenyl twisting motions herein.

To support the τ_2 assignment to the peripheral phenyl ring planarization, control experiments were performed on solvated ligands in multiple solvents using glycerol (20% by volume) to adjust viscosity.[47] The fitting results of fs-TA spectra show a clear lengthening of τ_2 and τ_3 from ~350 fs and 9 ps in DMSO to ~2 and 31 ps in DMSO+glycerol mixture (see Table 1; Fig. S4e, h, i), corroborating a slower twist and subsequent relaxation of the ligand in a more viscous solvent. We note that lengthening of the twisting time constant also reflects the enhanced H-bonding between glycerol and the benzoic acid groups. With the addition of glycerol, τ_2 matches the solvation time

of DMSO (~2 ps)[40] which is consistent with a dependence on solvent reorganization for ring-twisting motions, enforced by H-bonding with the peripheral acid groups (Fig. 1a). Furthermore, fs-TA spectra of water+glycerol mixture reveal a largely invariant τ_2 (~1 ps) but a substantially prolonged τ_3 from 6 ps in water (Fig. 3a) to 11.5 ps in the more viscous solvent (also see Fig. S4f for the probe-dependent fits in the SE peak region). This ~90% increase in τ_3 is consistent with the kinematic viscosity change from 0.960 in water to 1.776 ($\times 10^{-6}$ $m^2 \cdot s^{-1}$) in the water+glycerol mixture at 22 °C (lab room temperature), representing an 85% increase. Therefore, both H-bonding interactions and viscosity can slow the ultrafast twisting coordinate (τ_2) while viscosity mainly governs the subsequent relaxation (τ_3) of the linker in solution.

2.3. Ground-state FSRS reveals TBAPy vibrational signatures in different environments

The altered structures between the Al- and Sc-TBAPy MOFs have a profound impact on their photophysical properties and photocatalytic performance. To further this in-depth investigation, we performed GS- and ES-FSRS on the suspended MOFs, using solvated ligands as controls, since FSRS technique has showcased its power for exposing the structure-function relationships in a wide range of complex molecular systems in solution[39,48-50] and solid state.[45,51-54] The GS-FSRS spectra of TBAPy ligands are dominated by two bands at ~1267 and 1617 cm^{-1} (Fig. 4c), which closely match the free ligand spectra calculated using DFT method and the previously reported surface-enhanced stimulated Raman spectra for another TBAPy-based MOF (Fig. 4b).[55] These two bands involve stretching modes of the C–C and C=C bonds, respectively. In particular, the 1267 cm^{-1} peak contains a single normal mode, primarily a stretching motion along the short axis of the ligand and scissoring of the core hydrogens (Fig. S6a). The 1617 cm^{-1} mode is comprised of four calculated modes at ~1609, 1622, 1623 and 1652 cm^{-1} which can be respectively assigned

to core stretching along the short axis, symmetric and asymmetric stretching of the peripheral phenyl rings, and core stretching along the long axis (see Table 2 and Fig. S6e).

The notable parallels between the solvated ligands (pH 12) and Sc-TBAPy as well as the aggregated ligands (pH 3) and Al-TBAPy (see Fig. 4c) reinforce the fs-TA results (Fig. 2). In particular, Al-TBAPy and the aggregated ligands show blue-shifted Raman peaks with moderately dispersive lineshapes, likely due to resonance effects with respect to S_0 absorption bands;[56,57] for aggregated ligands, the red-shifted dimer absorption peaks at ~450 and 490 nm (Fig. S2a) could contribute with 540 nm Raman pump. The similarities between Al-TBAPy and aggregated ligands suggest that Al-TBAPy can form dimers in S_0 (i.e., a much looser one with ~7 Å interchromophoric distances[4,31] compared to ~3 Å in pure pyrene/TBAPy dimers);[27] other prominent modes appear between ca. 1100–1200 and 1400–1600 cm^{-1} (see green and blue traces in Fig. 4c).

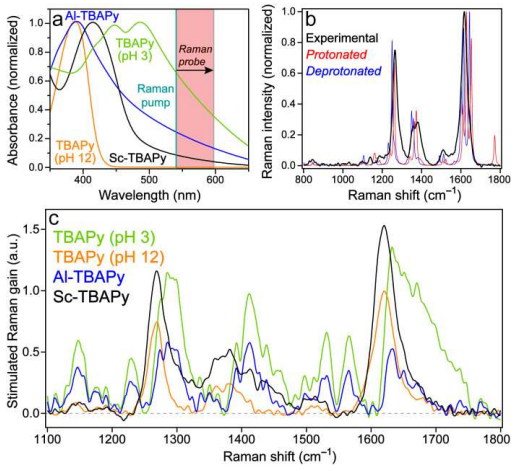

FIG. 4. Electronic and vibrational characterization of TBAPy ligands and MOFs in aqueous solution. (a) UV-visible absorption spectra of the concentrated ligand and MOF samples for FSRS experiments are shown for clarity of resonance conditions with 540 nm Raman pump (cyan vertical line) and Raman probe region (red shade) on the Stokes side. (b) The ground-state (GS)-FSRS

spectrum of TBAPy in pH 12 aqueous solution (black) is compared with the calculated Raman spectra of the protonated ligand (H_4TBAPy, red) and deprotonated ligand ($TBAPy^{4-}$, blue). (c) GS-FSRS spectra of Al-TBAPy (blue) and Sc-TBAPy (black) MOFs are compared with bare ligands in pH 3 (green) and 12 (orange) aqueous solution to show the characteristic peak patterns.

TABLE 2. Experimental and calculated Raman mode frequencies for TBAPy ligands in S_0.

FSRS experimental frequency (cm^{-1}) [a]	H_4TBAPy *in vacuo* (cm^{-1})	$TBAPy^{4-}$ *in vacuo* (cm^{-1}) [b]	$TBAPy^{4-}$ in water (cm^{-1}) [c]
1267	1268	1256	1255
1360	1371	1355	1356
1380	1381	1366	1366
1511	1530	1519	1519
1617	1618, 1636, 1638, 1661	1609, 1622, 1623, 1652	1608, 1624, 1624, 1650

[a] Ground-state (GS) data of bare ligands from Figs. 4c and 5b. [b] GS Raman modes from DFT calculations, scaled by 0.97, as shown in Fig. S6. [c] See more details in Supplementary Materials.

As for Sc-TBAPy, the observed Raman peaks have almost completely absorptive lineshapes (Fig. 4c) despite its ground-state absorption peak appearing redder than Al-TBAPy (Fig. 5a), so the low-energy absorption features in Al-TBAPy are not present in Sc-TBAPy. Neither MOF shows electronic absorption peaks of dimers (Figs. 1c, 4a, and S2b); however, both the negative peaks observed in fs-TA and the broadened, somewhat dispersive GS-FSRS peaks of Al-TBAPy strongly hint that dimers are present in the ground state, which also participate in the photoreaction pathways of Al-TBAPy. Moreover, these dimeric ligand states seem to compete with rather than enhance photocatalysis, accounting in part for the lower performance of Al-TBAPy. The relatively weak ground-state absorption of these dimers, due to their clearly reduced oscillator strength,[27,54] is likely obscured by the strong scattering background of the suspended MOFs in solution. This significant structural difference between these two MOFs is, at least in part, responsible for the markedly different excited-state properties and the higher photocatalytic efficiency of Sc-TBAPy.

2.4. Excited-state FSRS captures an ultrafast TBAPy ring-twisting event toward the CT state

To determine how molecular structural dynamics influence the excited-state relaxation of Sc-TBAPy vs. bare ligands, ES-FSRS affords a unique experimental window. In Fig. 5, the baseline-subtracted (see raw data and baselines in Fig. S7) ES-FSRS spectra of Sc-TBAPy (pH 7) and bare ligands in basic aqueous solution (pH 12) provide deep mechanistic insights. Strikingly, despite the similar GS-FSRS spectra of Sc-TBAPy and bare ligands (Fig. 4c), there are notable differences in the frequencies and dynamics of ES-FSRS peaks. Both samples exhibit two strong bands around 1267 and 1617 cm^{-1} in the ground state (S_0). However, bare ligands show a large blueshift of the 1267 cm^{-1} mode to ~1299 cm^{-1}, along with a small blueshift of the 1617 cm^{-1} mode to the excited state ($S_0 \rightarrow S_1$, Fig. 5b). In contrast, the corresponding S_1 modes in Sc-TBAPy appear at ~1293 and 1605 cm^{-1}, respectively (Fig. 5a). Moreover, bare ligands show low-frequency modes between 630–750 cm^{-1} (Fig. 5b; negative peaks are due to different resonance conditions versus the positive peaks for high-frequency modes, also see Fig. S7b)[36,58] which are not observed for Sc-TBAPy (Fig. 5a), indicative of the associated delocalized skeletal motions (with their dynamics reporting on structural deformations in a photoexcited state as the system undergoes ultrafast relaxation) of TBAPy ligands that become inhibited by the relatively rigid environment inside the framework.

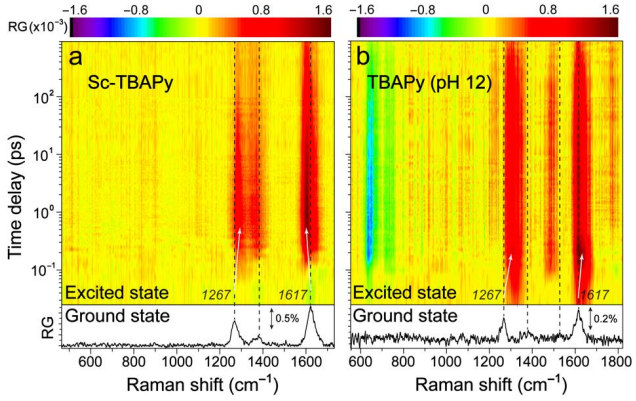

FIG. 5. Transient structural dynamics of TBAPy after 400 nm excitation. Semilogarithmic plots of the excited-state (ES)-FSRS data of (a) Sc-TBAPy MOF suspended in pH 7 aqueous solution and (b) bare TBAPy ligands in pH 12 aqueous solution, with 616 nm Raman pump and a redder probe for data collection on the Stokes side. The ground-state (GS)-FSRS spectra acquired throughout the ES-FSRS experiments are displayed in bottom panels with the stimulated Raman gain (RG) magnitude denoted by the double-headed arrow. Vertical dashed lines denote the ground-state marker bands so the excited-state peak frequency shifts (if applicable) are visible.

These characteristic Raman peak frequency shifts (from S_0 to S_1) reflect electron redistribution upon photoexcitation into the Franck-Condon region (i.e., $\pi \rightarrow \pi^*$). Ligand frontier molecular orbitals (HOMO→LUMO) electron density plots obtained from time-dependent (TD)-DFT calculations reveal a ~90° shift in the π-orbitals which are parallel with the long axis of the ligand pyrene core in S_0 and nearly parallel with the short axis in S_1 (Fig. S8). This result rationalizes the observed frequency shifts: stretching modes along the long axis are weakened and undergo a frequency redshift, while stretching modes primarily along the short axis are blue-shifted. For instance, the bridging C–C modes (~1267 and 1617 cm^{-1}) exhibit a blueshift from the ground to excited state for bare TBAPy ligands in pH 12 aqueous solution (Fig. 5b), which matches what we expect given the calculated HOMO/LUMO electron density maps of the deprotonated ligand with bonding character across the C–C bridge in LUMO (Fig. S8a). In addition, TD-DFT suggests an increased intramolecular charge transfer (ICT, or charge-separated/CS) character in the S_1 state of protonated H_4TBAPy, used as an economical model for the bound ligands within the MOF,[13,43] compared with the deprotonated chromophore $TBAPy^{4-}$ since the peripheral benzoate group can be considered as a weaker electron acceptor than the neutral benzoic acid (see Supplemental Materials, Fig. S8).

Notably, the excited-state Raman peak intensity dynamics of bare ligands (see Fig. 6b) mirror the fs-TA results (Figs. 2 and 3) with an ultrafast ~200 fs decay followed by a ~1.4 ps rise, and three decay components with time constants of ~7, 400, and 1900 ps. The dynamics are qualitatively identical for the ~1297 and 1614 cm^{-1} modes with only slight differences in the amplitude weight of each component. In conjunction with fs-TA results (Figs. 2 and 3), the initial decay is likely due to electronic redistribution out of the Franck-Condon region, while the 1.2–1.4 ps component tracks twisting of the phenyl groups, hindered by the solvation time of water.[35,36,40] The ~6–7 ps core deformation is followed by large-scale conformational change on the hundreds of ps timescale, ultimately terminating with a ~2 ns apparent fluorescence lifetime of the ligand.

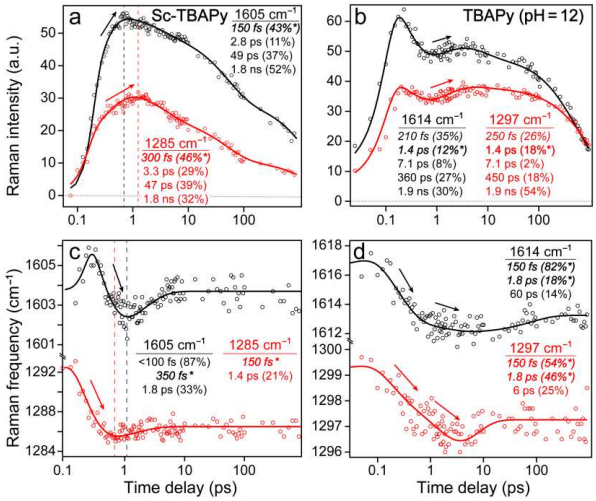

FIG. 6. Structural dynamics of the TBAPy ligand in contrasting environments. Excited-state (ES)-FSRS mode (a and b) intensity and (c and d) center frequency dynamics for two marker bands of Sc-TBAPy MOF suspended in pH 7 aqueous solution and bare ligands in pH 12 aqueous solution after 400 nm excitation. The least-squares fitted time constants and amplitude weights are listed for the ~1285/1297 cm^{-1} (red) and 1605/1614 cm^{-1} (black) modes. The color-coded vertical dashed

lines for Sc-TBAPy highlight different onset dynamics between two modes. The horizontal dotted lines represent zero Raman intensity. The peak intensity decay components have the combined amplitude weights of 100%, while the rise component with the proportional weight (scaled to the summation of all decay components) is bolded italic and denoted by an asterisk (also indicated by the color-coded arrows by data traces) in panels a and b. The peak frequency redshift component(s) have the combined weights of 100% and are bolded italic and denoted by an asterisk (also indicated by the color-coded arrows by data traces) in panels c and d. Meanwhile, the blueshift component(s) have the proportional weight that is each scaled to the summation of all the redshift components.

Importantly, the 1.4 ps solvation and phenyl ring-twisting component is associated with a rise of the excited-state mode intensity (Fig. 6b). This result is consistent with a rising 700 nm ESA band on the ~1.2 ps timescale (Fig. 3a) that achieves enhanced resonance with the probe pulse.[59,60] This explanation does not, however, account for the observation that the amplitude weight of the rise is greater for the 1297 cm^{-1} mode (with a corresponding Raman probe at ~669 nm) than for the 1614 cm^{-1} mode with Raman probe at ~684 nm. This key comparison contradicts the improved resonance enhancement as the sole origin for this rise. If this were the case, the 1614 cm^{-1} mode should see the greatest resonance enhancement due to its closeness to the rising 700 nm ESA peak as well as a continued rise with the ~7 ps component as shown by fs-TA results (see Fig. 3a).

Instead, this vibrational signature is rationalizable by the aforementioned planarization on this timescale which can enhance electronic delocalization across the pyrene-benzene bridge, thus increasing polarizability of Raman modes that involve the bridge C–C bond stretch (Fig. S6).[41,42,61] Meanwhile, the steric restriction imposed by the neighboring pyrene core and peripheral phenyl hydrogens should force the bridging C–C bond to lengthen, thus red-shifting the frequencies of

any stretching modes for this bond;[61] this is corroborated by the observed peak frequency dynamics on the pertinent timescale (Fig. 6d). On the other hand, simple solvation of the excited state would lead to a blueshift of the mode frequencies.[35] Both marker bands display a clear redshift on sub-ps and ~1.8 ps timescales, confirming the assignment of this ps time constant (slightly lengthened versus 1.4 ps in mode intensity dynamics) to a solvent-involved planarization step. Furthermore, the low-frequency and ~1500 cm^{-1} modes, which do not involve the bridge stretching, exhibit clear frequency blueshifts starting from time zero, likely tracking vibrational cooling events (Fig. S9).

Interestingly, Sc-TBAPy displays strikingly different excited-state Raman mode intensity and frequency dynamics (Fig. 6a, c) versus bare ligands (Fig. 6b, d). A clear initial rise for both marker bands with time constants of ~150 and 300 fs for the 1605 and 1285 cm^{-1} modes, respectively, is followed by three decay time constants of ~3, 50, and 1800 ps, in good agreement with fs-TA results (Fig. 3c). We note that the broad ESA band of Sc-TBAPy shows an initial rise on the <100 fs timescale, then decays monotonically toward zero which includes the 350 fs component. This finding indicates that the observed Raman intensity rise on the sub-ps timescale cannot be attributed to an improved dynamic resonance condition.[59] On the same timescale, the two marker bands manifest contrasting frequency dynamics: the ~1285 cm^{-1} mode shows a pronounced redshift of ~8 cm^{-1}, twice that observed for the free ligand (see red traces in Fig. 6c, d). The ~1605 cm^{-1} band, on the other hand, initially displays a small blueshift, followed by a larger redshift of ~4 cm^{-1} on the ~350 fs timescale (black trace, Fig. 6c). Notably, there is a clear difference between the local environments of the core and periphery groups within the MOF that is not present in bare/free ligands, causing the observed mode-specific dynamics after photoexcitation. Global analysis of the ES-FSRS spectra for TBAPy ligands in contrasting environments (Fig. S10) further retrieves key temporal components to corroborate these Raman signatures and characteristic shifts

for the later onset and a subsequent faster redshift of high-frequency modes in Sc-TBAPy than bare ligands in water (see Fig. 6).

We note that such useful information needs to be retrieved from ES-FSRS data, which provide deeper insights than a simple correlation or equivalence between the electronic and vibrational dynamics. For example, the fs-TA time constants of bare TBAPy ligands in pH 12 aqueous solution at the probe wavelengths corresponding to the ~1297 and 1614 cm^{-1} excited state modes (Fig. 6b) are similar to those shown in Fig. S4c (magenta trace above zero line for the ESA peak); however, notable differences exist in the ES-FSRS spectra capturing a 210–250 fs decay (vs. a <100 fs rise in TA) and a ~7 ps decay (vs. 6 ps rise in TA). Meanwhile, the difference between the observed electronic (TA) and vibrational (ES-FSRS) dynamics is more clear for Sc-TBAPy MOF, particularly for the ~350 fs decay in TA spectra (see Figs. 2c and 3c) vs. ~150–300 fs rise in ES-FSRS spectra (Fig. 6a) in the similar probe-wavelength region. Furthermore, the pertinent TD-DFT calculations for the fluorescent state (i.e., an optimized geometry in S_1) do predict an increase of the TBAPy ring planarity (with a ~10–15° twist of the peripheral rings) compared with the optimized ground state (S_0), indicative of the structural changes needed to go from the Franck-Condon region to the relaxed excited state, wherein we used ES-FSRS to experimentally capture important structural dynamics events on the sub-ps to ps timescales as highlighted in Fig. 6c, d.

On the basis of these excited-state vibrational signatures reporting on structural dynamics, key information can be deduced about the light-induced primary events. The substantially increased redshift of the core 1285 cm^{-1} mode of Sc-TBAPy MOF (compared to the free ligand in aqueous solution) results from both planarization and charge transfer away from the pyrene core, toward the peripheral phenyl groups and metal-ion nodes. This ultrafast CT process is reflected by the blueshift of the core-and-peripheral-ring mixed 1605 cm^{-1} mode (Fig. S6e) on the <100 fs

timescale (Fig. 6c), implying mixed contributions from the initial vibrational cooling out of the Franck-Condon region and some small-scale conformational motions across the ligand ring system.[35,36] Subsequently, the peripheral phenyl twisting occurs within a few hundred fs, which results in more substantial conformational changes and frequency redshifts of both marker bands (Fig. 6c); meanwhile, a continued intensity rise with peak frequency redshift can be seen for bare TBAPy ligands on the few ps timescale (Fig. 6d), implying that the more free surrounding solvent motions can augment the ring-twisting motions toward planarization.

As a result, the more "mundane" mode intensity decay and frequency blueshift occur after ~5 ps for free ligands in aqueous solution, yet after ~1 ps for confined ligands inside MOF. In the framework, the amount of internal water is much less than bulk water, and the degree of H-bonding with peripheral carboxylate groups is greatly reduced due to binding to metal ions, their dynamics and effects on the ligand vibrational features may also differ. Therefore, the incident light could promote a shorter yet more effective ligand planarization step which is captured by the prominent Raman peak intensity rise on the characteristic 150–300 fs timescale in Sc-TBAPy (Figs. 5a and 6a), in contrast to the earlier Raman peak onset for bare/free ligands in pH 12 water (Figs. 5b and 6b). These spectral distinctions shed important light on the initial excited-state relaxation pathways of TBAPy in different microscopic environments with water as a common player, which govern their macroscopic properties including the photocatalytic performance of M^{3+}-TBAPy MOFs. In addition, our recent work on a series of M^{3+}-TBAPy MOFs[28] has confirmed that both Sc- and Al-TBAPy MOFs maintain their crystallinity after photocatalysis, which strengthen their application prospects across various sustainable chemistry and energy fields.

Furthermore, on the molecular level, the 1285 cm^{-1} mode intensity peaks just after 1 ps, whereas the 1605 cm^{-1} mode peaks before 1 ps. Conversely, the 1605 cm^{-1} mode redshift

concludes slightly after 1 ps, yet before 1 ps for the 1285 cm^{-1} mode (see vertical dashed black and red lines in Fig. 6a, c). This seemingly intriguing result is fundamentally consistent with the delocalization of electron density from the ligand periphery, back to the pyrene core as the phenyl rings twist toward planarity in the MOF. In particular, DFT calculations corroborate the mode assignment that the 1285 cm^{-1} peak is more localized on the pyrene core (see the corresponding ground-state Raman mode in Fig. S6a), which reaches its intensity maximum later than the core-and-peripheral-ring mixed 1605 cm^{-1} mode (see the corresponding ground-state Raman modes in Fig. S6e). In essence, the ligand pyrene core acts as an intermediate "out-and-in" site with strong electronic and exchange coupling between the ligand donor and metal acceptor (where water molecules congregate)[13] in these frameworks for a transient CT process. Meanwhile, the mixed mode reaches its frequency redshift turning point later as both core and peripheral rings undergo the coordinated motions, as two connected moieties of TBAPy, to stabilize the nascent CT state (see Fig. 2c).[35,39] These results reveal the important role of this ultrafast twisting coordinate in governing the CT extent in Sc-TBAPy; following the initial CT reaction upon photoexcitation, planarization of the peripheral phenyl rings modulates the charge separation by controlling the degree of coupling between the donor and acceptor π systems. Moreover on the longer time scales and larger length scales, the photocatalytic activity of the materials necessitates electron transfer from the photoexcited ligands to the metal-ion nodes, and finally to the cocatalyst. This mechanism is reflected in the use of a CT state for describing the observed electronic species unique to these MOFs (Figs. 2, 3) which represents, at least, the early primary steps of this functional process.

2.5. Fs-TA spectra reveal altered ultrafast CT dynamics that underlie the glyphosate remedy

On the application front, Sc-TBAPy has been recently shown to facilitate H_2 generation from water under visible light illumination at considerably higher rates than other M^{3+}-TBAPy MOFs

(e.g., M = Al, Fe, Y). Moreover, Sc-TBAPy performs exceptionally well in both adsorption and photocatalytic degradation of the common pesticide glyphosate (GP)[28] at near-environmental concentrations, sequestering 100% of GP (1.5 mM aqueous solution) in five minutes, while involving non-toxic degradation pathways, therefore positioning it as a promising candidate for photocatalytic remediation of GP in natural systems. To delineate relevant steps toward photodegradation of GP, we performed fs-TA experiments on Sc-TBAPy immersed in 1.5 mM GP solution for a direct comparison with measurements in pH 7 water. Note that GP levels were measured up to 0.62 mM (105 ppm) in global freshwater systems,[62] so 1.5 mM (254 ppm) GP in water represents a relatively high-concentration case for MOF treatment, leading to more discernible spectral signals while maintaining practical relevance. Steady-state spectroscopy reveals a small redshift of the ground state absorption peak from 410 to 415 nm (~300 cm^{-1}) which likely results from the GP-adsorption process disrupting the water-lattice/water-ligand interactions (see Section 2.1 above) around Pore 2 in the framework (along the pyrene core long axis, see Fig. S1). Previous studies demonstrated the stability of Sc-TBAPy and related MOFs under similar conditions with constant visible irradiation.[12,13,22,63] The electronic absorption spectra collected by us before and after each fs-TA experiment confirm little to no MOF-degradation over the course.

Transient electronic spectra of Sc-TBAPy in the presence of GP show a reduced intensity, particularly within the CT band, accompanied by accelerated decay dynamics (Fig. 7a-d). The overall excited state lifetime, extracted from global analysis (Fig. S11), is substantially reduced from 6.7 ns in water to 4.8 ns in water with 1.5 mM GP, implying additional relaxation pathways introduced by GP in aqueous solution. The probe-dependent fitting of the CT peak intensity at ~590 nm (Fig. 7b) reveals highly similar time constants to neutral water; however, the decay amplitude weight on the ps timescale manifests a ~3-fold increase from 6% in water to 20% in GP

aqueous solution. As a nice control, the ~690 nm ESA peak dynamics are largely conserved, showing only slightly faster dynamics than neutral water case (Fig. 7d). These contrasting spectral signatures unveil how the rapidly adsorbed GP within Sc-TBAPy affects the initial CT population, accelerating subsequent relaxation of the MOF. Quenching of the excited state reveals direct interaction between GP and the photogenerated excitons, although the small changes to the 695 nm ESA band imply that GP does not greatly enhance the degree of CT formation (onset and magnitude, also see DADS plots in bottom panels of Fig. S11). Therefore, further optimization of the MOF properties for photocatalysis could involve an enhanced CT state with a more "balanced" formation and relaxation scheme within the framework to promote the excited-state functionality.

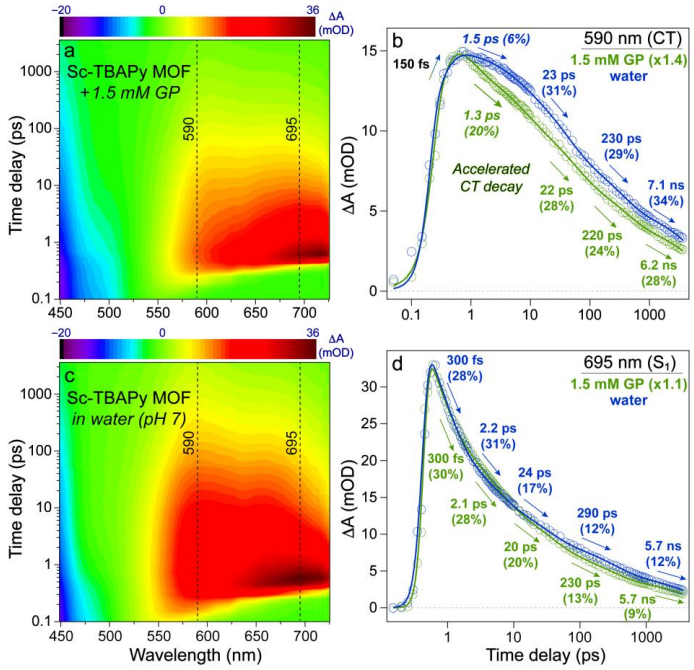

FIG. 7. Transient electronic dynamics of Sc-TBAPy MOF in the presence of photodegradation target glyphosate (GP). Contour plots of the fs-TA spectra of Sc-TBAPy MOF in (a) 1.5 mM GP

aqueous solution and (c) neutral water (pH 7) after 400 nm excitation. Peak intensity decay dynamics of the (b) ~590 nm CT band and (d) main 695 nm ESA band (data points in hollow circles) as denoted by vertical dashed lines in panels a and c, are plotted along with the least-squares fitting (color-coded solid lines) for both samples. The fitting time constants and their respective amplitude weights are included in the insets by the color-coded arrows: green, Sc-TBAPy + GP; blue, Sc-TBAPy only in neutral water.

Our research findings thus illuminate a pathway toward optimizing the photocatalytic performance through MOF-ligand functionalization. The addition of electron-withdrawing groups to the peripheral phenyl rings can promote directional intramolecular charge separation within the ligand. The steric restriction introduced by these groups could alter the equilibrium phenyl dihedral and nonequilibrium phenyl twisting that modifies the CT/CS magnitude and efficiency (which can motivate further investigations), while small changes to the ligand LUMO energy may increase mixing with the Sc *d*-orbitals. By way of caution, this strategy may not be the unmitigated success since the role of planarization for charge mobility in Sc-TBAPy requires further studies across a longer timescale, with a goal to evaluate the effects of restraining this twist coordinate on the effective/overall migration of charge carriers to support the downstream photocatalytic steps. The morphology of the resultant MOFs involving the size, shape, and facet may also play a role.[9,13] This current investigation on the photoinduced energy relaxation across fs-to-ns timescales of TBAPy ligands in water and MOFs offers an experimental platform and foundation to inspire future studies with substantial societal benefits for our fundamental understanding and practical applications of pyrene-based MOFs toward sustainable energy and green chemistry; therefore, it constitutes a great example for bridging the structure-function gap of novel engineerable materials.

Conclusions

In summary, we investigated transient electronic and vibrational characteristics of two isostructural MOFs with metal nodes, constructed from Sc^{3+} and Al^{3+} ions, connected via organic TBAPy linkers. Incorporation of the photoactive ligands within the frameworks facilitates ultrafast formation of a low-energy delocalized CT state in both MOFs upon a ligand-centered optical excitation; however, Sc-TBAPy exhibits substantially greater CT characters which result in the richer excited-state dynamics and higher photocatalytic efficiency, also with a redder absorption profile than Al-TBAPy. Global analysis of transient spectra of bare ligands and both MOFs in various solvents (pH 3, 7, and 12 aqueous solution) reveal a key sub-ps twist of the TBAPy peripheral phenyl groups, which appears to contribute to the CT efficiency of Sc-TBAPy. This represents a key finding about such a characteristic ring twist from this investigation: too much flexibility of the peripheral phenyl groups may enhance the nonradiative decay and quench the CT state, whereas too little flexibility may hinder the initial mobility of photogenerated excitons to enable the CT state on ultrafast timescales. Remarkably, excited-state FSRS measurements reveal two C–C/C=C stretching modes of the ligand which track this phenyl-ring twist in action in various environments, displaying a clear ultrafast frequency redshift in contrast to a common blueshift induced by vibrational cooling. Despite the similarity of ground-state FSRS spectra of Sc-TBAPy with bare ligands, the excited-state Raman mode frequencies of Sc-TBAPy are substantially shifted, which indicates an enhanced charge separation in the Sc framework.

Moreover, fs-TA measurements with global analysis of Sc-TBAPy in aqueous glyphosate (GP) solution (using a compact optical setup that is depicted in Fig. S12 to achieve an extended detection time window) exhibit an accelerated decay of the CT band within a few ps versus neutral water, which capture the previously hidden primary events governing the GP-photodegradation pathway.

Our results suggest that strategic ligand engineering (e.g., enhancing the push-pull mechanism via electron-donating/withdrawing groups while maintaining the peripheral ring planarization via steric hindrance) could enhance charge separation and directional energy transfer toward metal centers in similar Sc-pyrene MOFs. Our tunable FSRS investigation of these functional materials demonstrates the power of dynamic resonance Raman enhancement to capture real-time structural snapshots of light-induced processes in MOFs, particularly with appealing applications in aqueous solution like acting as a "herbicide terminator". Furthermore, our research findings about structural dynamics of Sc-TBAPy MOF on intrinsic molecular timescales governing its macroscopic photocatalytic functionality can directly illuminate the long sought-after structure-function relationships of photosensitive and/or photocontrollable systems. Therefore, we envision this work to motivate future studies and discoveries across the energy and sustainability-related disciplines of optomaterials, chemistry, physics, catalysis, and photosciences.

Supplementary Material

The supplementary material (SM) for this article is given via a link that connects the published paper with the associated SM, which includes the experimental and computational methods, supplementary Figures S1–S12 with additional discussions on M^{3+}-TBAPy MOFs (M=Sc, Al) and free ligands in various solvents and at different pH conditions (pH=3 and 12) with their distinct spectral features (i.e., steady-state electronic absorption, time-resolved electronic and vibrational spectra including fs-TA and FSRS) and scheme of the optical setup, and supplementary references.

ACKNOWLEDGMENTS

This research was funded by the U.S. National Science Foundation (NSF) grants CHE-2003550 and CBET-2038381 (to C.F.), and the Department of Chemistry at Oregon State University (OSU)

faculty start-up funding (to K.S.). This work was also partly supported by the OSU College of Science SciRIS-ii award grant (2022–2023) and Patricia Valian Reser Endowed Faculty Scholar Fund (2023–2026) to C.F. We acknowledge the OSU Department of Chemistry summer research fellowships (2022 and 2023, to L.S.L.).

AUTHOR DECLARATIONS

Conflict of Interest

The authors declare no conflict of interest.

Author Contributions

Logan Lancaster: Data curation (lead); Formal analysis (lead); Investigation (lead); Software (lead); Visualization (lead); Writing – original draft (lead). **Taylor Krueger:** Investigation (supporting); Methodology (supporting); Validation (supporting); Writing – original draft (supporting). **Cheng Chen:** Investigation (supporting); Methodology (supporting); Writing – review & editing (supporting). **Emmanuel Musa:** Investigation (supporting); Methodology (supporting); Writing – review & editing (supporting). **Jacob Lessard:** Investigation (supporting); Methodology (supporting); Writing – review & editing (supporting). **Nan-Chieh Chiu:** Investigation (supporting); Methodology (supporting); Writing – review & editing (supporting). **Makenzie Nord:** Investigation (supporting); Methodology (supporting). **Kyriakos Stylianou:** Conceptualization (supporting); Funding acquisition (supporting); Investigation (supporting); Resources (supporting); Writing – review & editing (supporting). **Chong Fang:** Conceptualization (lead); Funding acquisition (lead); Investigation (supporting); Project administration (lead); Resources (lead); Supervision (lead); Validation (lead); Visualization (supporting); Writing – review & editing (lead).

DATA AVAILABILITY

The data that support the findings of this study are present in the paper and the Supplementary Materials, and are available from the corresponding author upon reasonable request.

REFERENCES

[1]S. M. Moosavi, A. Nandy, K. M. Jablonka, D. Ongari, J. P. Janet, P. G. Boyd, Y. Lee, B. Smit, and H. J. Kulik. Understanding the diversity of the metal-organic framework ecosystem. *Nat. Commun.* **11**, 4068 (2020).

[2]S. Majumdar, S. M. Moosavi, K. M. Jablonka, D. Ongari, and B. Smit. Diversifying databases of metal organic frameworks for high-throughput computational screening. *ACS Appl. Mater. Interfaces* **13**, 61004-61014 (2021).

[3]K. C. Stylianou, R. Heck, S. Y. Chong, J. Bacsa, J. T. A. Jones, Y. Z. Khimyak, D. Bradshaw, and M. J. Rosseinsky. A guest-responsive fluorescent 3D microporous metal−organic framework derived from a long-lifetime pyrene core. *J. Am. Chem. Soc.* **132**, 4119-4130 (2010).

[4]S. Sudan, A. Gładysiak, B. Valizadeh, J.-H. Lee, and K. C. Stylianou. Sustainable capture of aromatic volatile organic compounds by a pyrene-based metal–organic framework under humid conditions. *Inorg. Chem.* **59**, 9029-9036 (2020).

[5]N.-C. Chiu, M. T. Nord, L. Tang, L. S. Lancaster, J. S. Hirschi, S. K. Wolff, E. M. Hutchinson, K. A. Goulas, W. F. Stickle, T. J. Zuehlsdorff, C. Fang, and K. C. Stylianou. Designing dual-functional metal–organic frameworks for photocatalysis. *Chem. Mater.* **34**, 8798–8807 (2022).

[6]L. Gan, M. T. Nord, J. M. Lessard, N. Q. Tufts, A. Chidambaram, M. E. Light, H. Huang, E. Solano, J. Fraile, F. Suárez-García, C. Viñas, F. Teixidor, K. C. Stylianou, and J. G. Planas. Biomimetic photodegradation of glyphosate in carborane-functionalized nanoconfined spaces. *J. Am. Chem. Soc.* **145**, 13730-13741 (2023).

[7]V. A. Milichko, S. V. Makarov, A. V. Yulin, A. V. Vinogradov, A. A. Krasilin, E. Ushakova, V. P. Dzyuba, E. Hey-Hawkins, E. A. Pidko, and P. A. Belov. Van der waals metal-organic framework as an excitonic material for advanced photonics. *Adv. Mater.* **29**, 1606034 (2017).

[8]J.-H. Qin, Y.-D. Huang, Y. Zhao, X.-G. Yang, F.-F. Li, C. Wang, and L.-F. Ma. Highly dense packing of chromophoric linkers achievable in a pyrene-based metal–organic framework for photoelectric response. *Inorg. Chem.* **58**, 15013-15016 (2019).

[9]J. Yu, R. Anderson, X. Li, W. Xu, S. Goswami, S. S. Rajasree, K. Maindan, D. A. Gómez-Gualdrón, and P. Deria. Improving energy transfer within metal–organic frameworks by aligning linker transition dipoles along the framework axis. *J. Am. Chem. Soc.* **142**, 11192-11202 (2020).

[10]S. Goswami, J. Yu, S. Patwardhan, P. Deria, and J. T. Hupp. Light-harvesting "antenna" behavior in NU-1000. *ACS Energy Lett.* **6**, 848-853 (2021).

[11]S. S. Rajasree, J. Yu, S. M. Pratik, X. Li, R. Wang, A. S. Kumbhar, S. Goswami, C. J. Cramer, and P. Deria. Superradiance and directional exciton migration in metal–organic frameworks. *J. Am. Chem. Soc.* **144**, 1396-1406 (2022).

[12]A. Cadiau, N. Kolobov, S. Srinivasan, M. G. Goesten, H. Haspel, A. V. Bavykina, M. R. Tchalala, P. Maity, A. Goryachev, A. S. Poryvaev, M. Eddaoudi, M. V. Fedin, O. F. Mohammed, and J. Gascon. A titanium metal–organic framework with visible-light-responsive photocatalytic activity. *Angew. Chem. Int. Ed.* **59**, 13468-13472 (2020).

[13]F. P. Kinik, A. Ortega-Guerrero, F. M. Ebrahim, C. P. Ireland, O. Kadioglu, A. Mace, M. Asgari, and B. Smit. Toward optimal photocatalytic hydrogen generation from water using pyrene-based metal–organic frameworks. *ACS Appl. Mater. Interfaces* **13**, 57118-57131 (2021).

[14]M. Gutierrez, B. Cohen, F. Sánchez, and A. Douhal. Photochemistry of Zr-based MOFs: Ligand-to-cluster charge transfer, energy transfer and excimer formation, what else is there? *Phys. Chem. Chem. Phys.* **18**, 27761-27774 (2016).

[15]Y. Zhang, J. Guo, L. Shi, Y. Zhu, K. Hou, Y. Zheng, and Z. Tang. Tunable chiral metal organic frameworks toward visible light–driven asymmetric catalysis. *Sci. Adv.* **3**, e1701162 (2017).

[16]Q. L. Guan, Y. H. Xing, J. Liu, C. Han, C. Y. Hou, and F. Y. Bai. Bismuth-carboxylate ligand 1,3,6,8-tetrakis(*p*-benzoic acid)pyrene frameworks, photophysical properties, biological imaging, and fluorescent sensor for biothiols. *J. Phys. Chem. C* **123**, 23287-23296 (2019).

[17]M. Raytchev, E. Pandurski, I. Buchvarov, C. Modrakowski, and T. Fiebig. Bichromophoric interactions and time-dependent excited state mixing in pyrene derivatives. A femtosecond broad-band pump−probe study. *J. Phys. Chem. A* **107**, 4592-4600 (2003).

[18]S. Bernhardt, M. Kastler, V. Enkelmann, M. Baumgarten, and K. Müllen. Pyrene as chromophore and electrophore: Encapsulation in a rigid polyphenylene shell. *Chem. Eur. J.* **12**, 6117-6128 (2006).

[19]J. Sung, P. Kim, Y. O. Lee, J. S. Kim, and D. Kim. Characterization of ultrafast intramolecular charge transfer dynamics in pyrenyl derivatives: Systematic change of the number of peripheral *N*,*N*-dimethyaniline substituents. *J. Phys. Chem. Lett.* **2**, 818-823 (2011).

[20]T. D. Krueger, S. A. Boulanger, L. Zhu, L. Tang, and C. Fang. Discovering a rotational barrier within a charge-transfer state of a photoexcited chromophore in solution. *Struct. Dyn.* **7**, 024901 (2020).

[21]B. V. Kramar, B. T. Phelan, E. A. Sprague-Klein, B. T. Diroll, S. Lee, K.-i. Otake, R. Palmer, M. W. Mara, O. K. Farha, J. T. Hupp, and L. X. Chen. Single-atom metal oxide sites as traps for charge separation in the zirconium-based metal–organic framework NDC–NU-1000. *Energy Fuels* **35**, 19081-19095 (2021).

[22]Y. Xiao, J. Liu, J. Leng, Z. Yin, Y. Yin, F. Zhang, C. Sun, and S. Jin. Long-lived internal charge-separated state in two-dimensional metal–organic frameworks improving photocatalytic performance. *ACS Energy Lett.* **7**, 2323-2330 (2022).

[23]P. Deria, J. Yu, T. Smith, and R. P. Balaraman. Ground-state versus excited-state interchromophoric interaction: Topology dependent excimer contribution in metal–organic framework photophysics. *J. Am. Chem. Soc.* **139**, 5973-5983 (2017).

[24]A. Van Wyk, T. Smith, J. Park, and P. Deria. Charge-transfer within Zr-based metal–organic framework: The role of polar node. *J. Am. Chem. Soc.* **140**, 2756-2760 (2018).

[25]J. Yu, J. Park, A. Van Wyk, G. Rumbles, and P. Deria. Excited-state electronic properties in Zr-based metal–organic frameworks as a function of a topological network. *J. Am. Chem. Soc.* **140**, 10488-10496 (2018).

[26]K. Maindan, X. Li, J. Yu, and P. Deria. Controlling charge-transport in metal–organic frameworks: Contribution of topological and spin-state variation on the iron–porphyrin centered redox hopping rate. *J. Phys. Chem. B* **123**, 8814-8822 (2019).

[27]R. D. Pensack, R. J. Ashmore, A. L. Paoletta, and G. D. Scholes. The nature of excimer formation in crystalline pyrene nanoparticles. *J. Phys. Chem. C* **122**, 21004-21017 (2018).

[28]N.-C. Chiu, J. M. Lessard, E. N. Musa, L. S. Lancaster, C. Wheeler, T. D. Krueger, C. Chen, T. C. Gallagher, M. T. Nord, H. Huang, P. H.-Y. Cheong, C. Fang, and K. C. Stylianou.

Elucidation of the role of metals in the adsorption and photodegradation of herbicides by metal-organic frameworks. *Nat. Commun.*, **15**, 1459 (2024).

[29]T. Oyamada, S. Akiyama, M. Yahiro, M. Saigou, M. Shiro, H. Sasabe, and C. Adachi. Unusual photoluminescence characteristics of tetraphenylpyrene (TPPY) in various aggregated morphologies. *Chem. Phys. Lett.* **421**, 295-299 (2006).

[30]S. Yamaguchi, I. Yoshikawa, T. Mutai, and K. Araki. Solid-state luminescence of tetraphenylpyrene derivatives: Mechano/vapochromic luminescence of 1,3,6,8-tetra(4′-carboxyphenyl)pyrene. *J. Mater. Chem.* **22**, 20065-20070 (2012).

[31]P. G. Boyd, A. Chidambaram, E. García-Díez, C. P. Ireland, T. D. Daff, R. Bounds, A. Gładysiak, P. Schouwink, S. M. Moosavi, M. M. Maroto-Valer, J. A. Reimer, J. A. R. Navarro, T. K. Woo, S. Garcia, K. C. Stylianou, and B. Smit. Data-driven design of metal–organic frameworks for wet flue gas CO_2 capture. *Nature* **576**, 253-256 (2019).

[32]S. Shirai, and S. Inagaki. *Ab initio* study on the excited states of pyrene and its derivatives using multi-reference perturbation theory methods. *RSC Adv.* **10**, 12988-12998 (2020).

[33]Q. Zhou, Y. Guo, and Y. Zhu. Photocatalytic sacrificial H_2 evolution dominated by micropore-confined exciton transfer in hydrogen-bonded organic frameworks. *Nat. Catal.* **6**, 574-584 (2023).

[34]V. S. Vyas, S. V. Lindeman, and R. Rathore. Photophysical properties of 1,3,6,8-tetraarylpyrenes and their cation radicals. *J. Photochem. Photobiol. A* **375**, 209-218 (2019).

[35]T. Kumpulainen, B. Lang, A. Rosspeintner, and E. Vauthey. Ultrafast elementary photochemical processes of organic molecules in liquid solution. *Chem. Rev.* **117**, 10826-10939 (2017).

[36]C. Fang, L. Tang, and C. Chen. Unveiling coupled electronic and vibrational motions of chromophores in condensed phases. *J. Chem. Phys.* **151**, 200901 (2019).

[37]N. Agmon, D. Huppert, A. Masad, and E. Pines. Excited-state proton-transfer to methanol water mixtures. *J. Phys. Chem.* **95**, 10407-10413 (1991).

[38]F. Han, W. Liu, and C. Fang. Excited-state proton transfer of photoexcited pyranine in water observed by femtosecond stimulated Raman spectroscopy. *Chem. Phys.* **422**, 204-219 (2013).

[39]L. Tang, L. Zhu, Y. Wang, and C. Fang. Uncovering the hidden excited state toward fluorescence of an intracellular pH indicator. *J. Phys. Chem. Lett.* **9**, 4969-4975 (2018).

[40]M. L. Horng, J. A. Gardecki, A. Papazyan, and M. Maroncelli. Subpicosecond measurements of polar solvation dynamics: Coumarin 153 revisited. *J. Phys. Chem.* **99**, 17311-17337 (1995).

[41]P. Roy, A. Jha, V. B. Yasarapudi, T. Ram, B. Puttaraju, S. Patil, and J. Dasgupta. Ultrafast bridge planarization in donor-π-acceptor copolymers drives intramolecular charge transfer. *Nat. Commun.* **8**, 1716 (2017).

[42]S. Kayal, K. Roy, and S. Umapathy. Femtosecond coherent nuclear dynamics of excited tetraphenylethylene: Ultrafast transient absorption and ultrafast Raman loss spectroscopic studies. *J. Chem. Phys.* **148**, 024301 (2018).

[43]Z. Piontkowski, and D. W. McCamant. Excited-state planarization in donor–bridge dye sensitizers: Phenylene versus thiophene bridges. *J. Am. Chem. Soc.* **140**, 11046-11057 (2018).

[44]T. D. Krueger, G. Giesbers, R. C. Van Court, L. Zhu, R. Kim, C. M. Beaudry, S. C. Robinson, O. Ostroverkhova, and C. Fang. Ultrafast dynamics and photoresponse of a fungi-derived pigment xylindein from solution to thin films. *Chem. Eur. J.* **27**, 5627-5631 (2021).

[45]M. J. Hong, L. Zhu, C. Chen, L. Tang, Y.-H. Lin, W. Li, R. Johnson, S. Chattopadhyay, H. J. Snaith, C. Fang, and J. G. Labram. Time-resolved changes in dielectric constant of metal halide perovskites under illumination. *J. Am. Chem. Soc.* **142**, 19799-19803 (2020).

[46]S. Y. Kwang, and R. R. Frontiera. Spatially offset femtosecond stimulated Raman spectroscopy: Observing exciton transport through a vibrational lens. *J. Phys. Chem. Lett.* **11**, 4337-4344 (2020).

[47]J. B. Segur, and H. E. Oberstar. Viscosity of glycerol and its aqueous solutions. *Ind. Eng. Chem.* **43**, 2117-2120 (1951).

[48]C. Fang, R. R. Frontiera, R. Tran, and R. A. Mathies. Mapping GFP structure evolution during proton transfer with femtosecond Raman spectroscopy. *Nature* **462**, 200-204 (2009).

[49]D. R. Dietze, and R. A. Mathies. Femtosecond stimulated Raman spectroscopy. *ChemPhysChem* **17**, 1224–1251 (2016).

[50]W. Liu, Y. Wang, L. Tang, B. G. Oscar, L. Zhu, and C. Fang. Panoramic portrait of primary molecular events preceding excited state proton transfer in water. *Chem. Sci.* **7**, 5484-5494 (2016).

[51]F. Provencher, N. Bérubé, A. W. Parker, G. M. Greetham, M. Towrie, C. Hellmann, M. Côté, N. Stingelin, C. Silva, and S. C. Hayes. Direct observation of ultrafast long-range charge separation at polymer-fullerene heterojunctions. *Nat. Commun.* **5**, 4288 (2014).

[52]A. E. Bragg, W. Yu, J. Zhou, and T. Magnanelli. Ultrafast Raman spectroscopy as a probe of local structure and dynamics in photoexcited conjugated materials. *J. Phys. Chem. Lett.* **7**, 3990-4000 (2016).

[53]A. A. Cassabaum, W. R. Silva, C. C. Rich, and R. R. Frontiera. Orientation and polarization dependence of ground- and excited-state FSRS in crystalline betaine-30. *J. Phys. Chem. C* **123**, 12563-12572 (2019).

[54]T. D. Krueger, and C. Fang. Elucidating inner workings of naturally sourced organic optoelectronic materials with ultrafast spectroscopy. *Chem. Eur. J.* **27**, 17736–17750 (2021).

[55]J. W. M. Osterrieth, D. Wright, H. Noh, C.-W. Kung, D. Vulpe, A. Li, J. E. Park, R. P. Van Duyne, P. Z. Moghadam, J. J. Baumberg, O. K. Farha, and D. Fairen-Jimenez. Core–shell gold nanorod@zirconium-based metal–organic framework composites as *in situ* size-selective Raman probes. *J. Am. Chem. Soc.* **141**, 3893-3900 (2019).

[56]A. Weigel, A. Dobryakov, B. Klaumünzer, M. Sajadi, P. Saalfrank, and N. P. Ernsting. Femtosecond stimulated Raman spectroscopy of flavin after optical excitation. *J. Phys. Chem. B* **115**, 3656-3680 (2011).

[57]C. Chen, L. Zhu, and C. Fang. Femtosecond stimulated Raman line shapes: Dependence on resonance conditions of pump and probe pulses. *Chin. J. Chem. Phys.* **31**, 492-502 (2018).

[58]C. Chen, W. Liu, M. S. Baranov, N. S. Baleeva, I. V. Yampolsky, L. Zhu, Y. Wang, A. Shamir, K. M. Solntsev, and C. Fang. Unveiling structural motions of a highly fluorescent superphotoacid by locking and fluorinating the GFP chromophore in solution. *J. Phys. Chem. Lett.* **8**, 5921–5928 (2017).

[59]B. G. Oscar, C. Chen, W. Liu, L. Zhu, and C. Fang. Dynamic Raman line shapes on an evolving excited-state landscape: Insights from tunable femtosecond stimulated Raman spectroscopy. *J. Phys. Chem. A* **121**, 5428-5441 (2017).

[60]C. Fang, L. Tang, B. G. Oscar, and C. Chen. Capturing structural snapshots during photochemical reactions with ultrafast Raman spectroscopy: From materials transformation to biosensor responses. *J. Phys. Chem. Lett.* **9**, 3253–3263 (2018).

[61]M. Zhou, K. Wang, Z. Men, S. Gao, Z. Li, and C. Sun. Study of high-pressure Raman intensity behavior of aromatic hydrocarbons: Benzene, biphenyl and naphthalene. *Spectrochim. Acta A* **97**, 526-531 (2012).

[62]E. M. Brovini, S. J. Cardoso, G. R. Quadra, J. A. Vilas-Boas, J. R. Paranaíba, R. d. O. Pereira, and R. F. Mendonça. Glyphosate concentrations in global freshwaters: Are aquatic organisms at risk? *Environ. Sci. Pollut. Res.* **28**, 60635-60648 (2021).

[63]E. N. Musa, S. Kaur, T. C. Gallagher, T. M. Anthony, W. F. Stickle, L. Árnadóttir, and K. C. Stylianou. Two birds, one stone: Coupling hydrogen production with herbicide degradation over metal–organic framework-derived titanium dioxide. *ACS Catal.* **13**, 3710-3722 (2023).